Research Article

Low-Speed Sensorless Control for the Interior Permanent Magnet Synchronous Motors with Sliding Discrete Fourier Transform

Wenbao Hou [iD],[1,2] **Guojun Tan** [iD],[1] **and Zang Ling**[1]

[1]*School of Electrical and Power Engineering, China University of Mining and Technology, Xuzhou, China*
[2]*Jiangsu Vocational Institute of Architectural Technology, Xuzhou, China*

Correspondence should be addressed to Guojun Tan; gjtan_cumt@163.com

An efficient estimation of the rotor position has always been a premise of the reliable operation for the interior permanent magnet synchronous motors (IPMSM), especially for low-speed conditions because of the small back electromotive force (EMF) and low signal-to-noise ratio (SNR). The commonly used observation method, e.g., sliding mode observer (SMO), is suitable for these surface mounted motors and has no great adaptability to the saliency. In this paper, a novel rotor position (including the real-time position and initial position) estimation method was proposed based on the traditional high-frequency signal injection method. Firstly, high-frequency signals were injected to induce the high-frequency current components which contain the rotor position information. Then, the sliding discrete Fourier transform (SDFT) algorithm was used to extract the amplitudes of the induced current components which could be used to get the real-time and initial rotor positions by a proportional integral (PI) regulator and a polarity identification. Lastly, with the established experiments' platform, the estimation tests of the rotor position at a low speed have been completed to make verification of the effectiveness of the approach studied in this paper.

1. Introduction

Permanent magnet synchronous motors (PMSMs) are widely used in industrial areas, e.g., manufactures, household appliances, transportation, or even aerospace field for their sorts of advantages [1–3]. An efficient acquisition of the rotor position has always being one of the preconditions to ensure the reliable operation. Normally, rotor position can be obtained by mechanical sensors, e.g., rotary or photoelectric encoders; however, these sensors usually need additional signal detection and processing, are sensitive to the environments, and are not suitable for all occasions. Therefore, it is an important research object of the study to develop the sensorless control [4–6].

Typically, there are three kinds of sensorless methods being widely studied for the rotor position estimation. (1) Methods based on the motor back EMF, e.g., sliding mode observer (SMO) and extended Kalman filter (EKF); however, these methods are usually suitable for surface mounted

motors and have no great adaptability to the saliency [7, 8]. (2) For IPMSMs, the common methods to estimate the rotor position are based on high-frequency signal injection because the position information would be contained in the induced signals [9–11]. Usually, signals' extraction can be carried out in the frequency domain, during which the discrete Fourier transform and its extension are preferred [12]. Considering that the calculation for the common discrete Fourier transform is relatively complicated, a generalized sliding discrete Fourier transform was proposed in [13, 14], which could improve the efficiency of signal extraction and was suitable for digital implementation. (3) Methods based on intelligent algorithms: for example, a novel speed observation scheme using artificial neural network inverse method was proposed in [15] to effectively reject the influence of speed detection on system stability and precision for the motor; in [16], an iterative search strategy based on dichotomy was proposed to provide a finite number of rotor position angles with good accuracy.

On the contrary, for IPMSMs, the initial rotor position information is also important for effectively starting up, which is different from the sensorless control of the induction motors (IMs). When the motor is stationary, the back EMF keeps zero which means it could not be used to get the initial position. Although the rotor initial position information exists in the induced high-frequency current components whether the motor is stop or in motion state, the N/S polarity of the rotor pole cannot be identified directly. In [17], a second-order Taylor expansion was adopted to extract the N/S poles, which was not suitable for the digital realization because of the complicated computation.

In order to effectively estimate the real-time and initial rotor positions for the IPMSMs, a novel estimation strategy was proposed in this paper based on the combination of high-frequency signal injection and the SDFT algorithm. Firstly, high-frequency voltages are injected to induce the high-frequency current components which contain the rotor position information. Then, the SDFT algorithm is used to make an effective signal extraction of the induced current components to ensure the real-time rotor position estimation. Meanwhile, a magnetic polarity identification method is designed to get the initial position according to the amplitude variation of the induced high-frequency current components.

This paper is organized as follows. The estimation strategy of the real-time rotor position is given in Section 2. The initial position judgment is presented in Section 3. The experimental results are shown in Section 4. Finally, some conclusions are given in Section 5.

2. Real-Time Estimation of Rotor Position

2.1. Estimation Principle. For the IPMSMs, the flux equations in dq coordinate can be expressed as

$$\begin{bmatrix} \Psi_d \\ \Psi_q \end{bmatrix} = \begin{bmatrix} L_d & 0 \\ 0 & L_q \end{bmatrix} \begin{bmatrix} i_d \\ i_q \end{bmatrix} + \begin{bmatrix} \Psi_f \\ 0 \end{bmatrix}, \tag{1}$$

where Ψ_d and Ψ_q are the stator fluxes in the dq coordinate, i_d and i_q are the stator currents in dq coordinate, L_d represents the inductance in direct axis while L_q is the inductance in quadrature axis, and Ψ_f stands for the permanent magnet excitation component.

Hypothesis is that a virtual rotating $d'q'$ coordinate whose relationship with the normal dq coordinate is revealed in Figure 1.

Defining the deviation of the two coordinates, $\Delta\theta = \theta - \theta'$, then the transform matrix between the normal and virtual rotating coordinates could be presented as

$$T_{d'q' \longrightarrow dq} = \begin{bmatrix} \cos\Delta\theta & \sin\Delta\theta \\ -\sin\Delta\theta & \cos\Delta\theta \end{bmatrix}. \tag{2}$$

With the high-frequency voltages being injected into the stator windings, the stator fluxes generated by the induced high-frequency current components can be described as
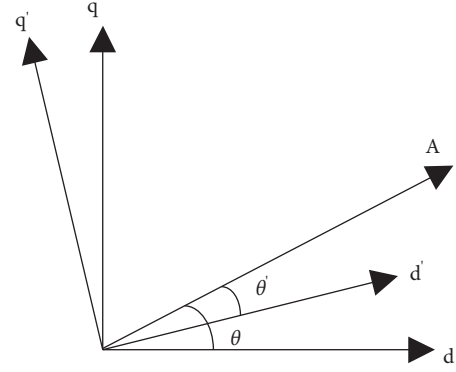

FIGURE 1: Relationship of the virtual and normal rotating coordinates, where θ is the rotor position angle between axis "d" and axis "A" (axis "A" is the a-phase winding in the three-phase stationary coordinates). θ' is the virtual angle between the axis "d'" and the axis "A."

$$\begin{bmatrix} \Psi_{id} \\ \Psi_{iq} \end{bmatrix} = \begin{bmatrix} L_d & 0 \\ 0 & L_q \end{bmatrix} \begin{bmatrix} i_{id} \\ i_{iq} \end{bmatrix}, \tag{3}$$

where Ψ_{id} and Ψ_{iq} are the generated flux components from the induced high-frequency current components in dq coordinates and i_{id} and i_{iq} are the corresponding induced high-frequency current components, respectively.

With the transform matrix, these generated flux components also could be written as

$$\begin{bmatrix} \Psi_{id} \\ \Psi_{iq} \end{bmatrix} = T_{d'q' \longrightarrow dq} \begin{bmatrix} \Psi_{id'} \\ \Psi_{id'} \end{bmatrix}. \tag{4}$$

Similarly, the induced high-frequency current components also could be described as

$$\begin{bmatrix} i_{id} \\ i_{iq} \end{bmatrix} = T_{d'q' \longrightarrow dq} \begin{bmatrix} i_{id'} \\ i_{iq'} \end{bmatrix}. \tag{5}$$

Substituting equations (3) and (5) into equation (4), then

$$T_{d'q' \longrightarrow dq} \begin{bmatrix} \Psi_{id'} \\ \Psi_{iq'} \end{bmatrix} = \begin{bmatrix} L_d & 0 \\ 0 & L_q \end{bmatrix} T_{d'q' \longrightarrow dq} \begin{bmatrix} i_{id'} \\ i_{iq'} \end{bmatrix}. \tag{6}$$

For equation (6), the induced current components in $d'q'$ coordinate can be obtained as

$$\begin{bmatrix} i_{id'} \\ i_{iq'} \end{bmatrix} = T_{d'q' \longrightarrow dq}^{-1} \begin{bmatrix} L_d & 0 \\ 0 & L_q \end{bmatrix}^{-1} T_{d'q' \longrightarrow dq} \begin{bmatrix} \Psi_{id'} \\ \Psi_{iq'} \end{bmatrix}$$

$$= \frac{1}{L_\Sigma^2 - L_\Delta^2} \begin{bmatrix} L_\Sigma + L_\Delta\cos(2\Delta\theta) & L_\Delta\sin(2\Delta\theta) \\ L_\Delta\sin(2\Delta\theta) & L_\Sigma - L_\Delta\cos(2\Delta\theta) \end{bmatrix}$$

$$\cdot \begin{bmatrix} \Psi_{id'} \\ \Psi_{iq'} \end{bmatrix}, \tag{7}$$

where $L_\Sigma = (L_d + L_q)/2$ and $L_\Delta = (L_q - L_d)/2$.

Suppose that the high-frequency voltage injected into the stator windings are as follows:

$$\begin{bmatrix} u_{id'} \\ u_{iq'} \end{bmatrix} = U_i \begin{bmatrix} \sin \omega_i t \\ \cos \omega_i t \end{bmatrix}. \tag{8}$$

With voltage-flux relationship, the generated flux components can be written as

$$\begin{bmatrix} \Psi_{id'} \\ \Psi_{iq'} \end{bmatrix} = \frac{U_i}{\omega_i} \begin{bmatrix} -\cos \omega_i t \\ \sin \omega_i t \end{bmatrix}. \tag{9}$$

Substituting equation (9) into equation (7), then

$$\begin{bmatrix} i_{id'} \\ i_{iq'} \end{bmatrix} = \frac{U_i}{\omega_i \left(L_\Sigma^2 - L_\Delta^2 \right)} \begin{bmatrix} L_\Sigma + L_\Delta \cos(2\Delta\theta) & L_\Delta \sin(2\Delta\theta) \\ L_\Delta \sin(2\Delta\theta) & L_\Sigma - L_\Delta \cos(2\Delta\theta) \end{bmatrix} \begin{bmatrix} -\cos \omega_i t \\ \sin \omega_i t \end{bmatrix}$$

$$= \frac{U_i}{\omega_i \left(L_\Sigma^2 - L_\Delta^2 \right)} \begin{bmatrix} -L_\Sigma \cos(\omega_i t) - L_\Delta \cos(2\Delta\theta)\cos \omega_i t + L_\Delta \sin(2\Delta\theta)\sin \omega_i t \\ -L_\Delta \sin(2\Delta\theta)\cos \omega_i t + L_\Sigma \sin \omega_i t - L_\Delta \cos(2\Delta\theta)\sin \omega_i t \end{bmatrix}. \tag{10}$$

The simplification of equation (10) can be derived as

$$\begin{cases} i_{id'} = -(I_{i0} + I_{i1} \cos(2\Delta\theta))\cos \omega_i t + I_{i1} \sin((2\Delta\theta))\sin \omega_i t, \\ i_{iq'} = -I_{i1} \sin(2\Delta\theta)\cos \omega_i t + (I_{i0} - I_{i1} \cos(2\Delta\theta))\sin \omega_i t, \end{cases} \tag{11}$$

where $I_{i0} = (U_i L_\Sigma / \omega_i (L_\Sigma^2 - L_\Delta^2))$ and $I_{i1} = (U_i L_\Delta / \omega_i (L_\Sigma^2 - L_\Delta^2))$.

The amplitudes of the induced high-frequency current components could be expressed and derived as

$$\begin{cases} \left| i_{id'} \right| = \sqrt{(I_{i0} + I_{i1} \cos(2\Delta\theta))^2 + (I_{i1} \sin(2\Delta\theta))^2} \\ \left| i_{iq'} \right| = \sqrt{(I_{i1} \sin(2\Delta\theta))^2 + (I_{i0} - I_{i1} \cos(2\Delta\theta))^2} \end{cases} \Rightarrow \begin{cases} \left| i_{id'} \right|^2 = I_{i0}^2 + I_{i1}^2 + 2I_{i1}I_{i0} \cos(2\Delta\theta) \\ \left| i_{iq'} \right|^2 = I_{i0}^2 + I_{i1}^2 - 2I_{i1}I_{i0} \cos(2\Delta\theta) \end{cases}. \tag{12}$$

Furthermore,

$$\left| i_{id'} \right|^2 - \left| i_{iq'} \right|^2 = 4I_{i1}I_{i0} \cos(2\Delta\theta). \tag{13}$$

It is obvious that there is a cosine component of the deviation angle $\Delta\theta$ in equation (13), which can be easily transformed into the sinusoidal component by changing the rotating transform equation (2) with a $(\pi/4)$ conversion such as

$$T_{d''q'' \longrightarrow d'q'} = \begin{bmatrix} \cos\left(\Delta\theta - \dfrac{\pi}{4}\right) & \sin\left(\Delta\theta - \dfrac{\pi}{4}\right) \\ -\sin\left(\Delta\theta - \dfrac{\pi}{4}\right) & \cos\left(\Delta\theta - \dfrac{\pi}{4}\right) \end{bmatrix}. \tag{14}$$

In the new $d''q''$ coordinate, equation (13) would be changed as

$$\left| i_{id''} \right|^2 - \left| i_{iq''} \right|^2 = 4I_{i1}I_{i0} \cos(2\Delta\theta') = 4I_{i1}I_{i0} \cos\left(2\left(\Delta\theta - \dfrac{\pi}{4}\right)\right)$$

$$= 4I_{i1}I_{i0} \sin(2\Delta\theta). \tag{15}$$

For equation (15), if the quantity of the left side is known, then the $2\Delta\theta$ could be adjusted to 0 by setting an appropriate PI regulator, which means virtual angle θ' equals the actual rotor position angle θ, that is, the real-time rotor position information.

2.2. Amplitudes' Extraction Based on SDFT.

SDFT is an improved algorithm for traditional discrete Fourier transform (DFT), which can greatly reduce the computational complexity and easily extract the amplitude of specific frequency signals.

Assume that the induced high-frequency current is a finite data sequence, which can be expressed as $i(m)$ and its length is M, and its DFT is

$$I(k) = DFT[i(m)] = \sum_{n=0}^{M-1} i(m)W_M^{nk}, \quad (0 \leq k \leq M - 1), \tag{16}$$

where $W_M = e^{(-j2\pi/M)}$.

For equation (16), its expansion can be mathematically expressed as

$$I(k) = i(0) + i(1)e^{-j(2\pi k/M)} + i(2)e^{-j(2\pi k*2/M)} + \ldots + i(M-1)e^{-j(2\pi k*(M-1)/M)}. \tag{17}$$

Suppose that the first sampling M data are $i(0) \sim i(M-1)$, and the first sequence is represented as i_0; the second sampling M data are $i(1) \sim i(M)$, and the corresponding sequence is i_1. The data processing is shown in Figure 2.

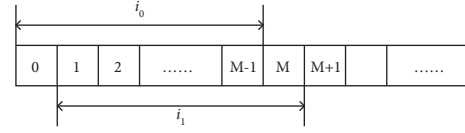Defining $I_0(k)$ and $I_1(k)$ are the DFT of the sequences i_0 and i_1, respectively,

FIGURE 2: Schematic diagram of discrete data processing.

$$I_0(k) = i(0) + i(1)e^{-j(2\pi k/M)} + i(2)e^{-j(2\pi k*2/M)} + \ldots + i(M-1)e^{-j(2\pi k*(M-1)/M)}, \tag{18}$$

$$I_1(k) = i(0) + i(1)e^{-j(2\pi k/M)} + i(3)e^{-j(2\pi k*2/M)} + \ldots + i(M)e^{-j(2\pi k*(M-1)/M)}, \tag{19}$$

Combining the above two equations, it could be derived as

$$\begin{aligned} I_1(k) &= [I_0(k) - i(0)]e^{j(2\pi k/M)} + i(M)e^{-j(2\pi k(M-1)/M)} \\ &= [I_0(k) - i(0) + i(M)]e^{j(2\pi k/M)}. \end{aligned} \tag{20}$$

Obviously, equation (20) shows that $I_1(k)$ can be calculated only by using $I_0(k)$, $i(0)$, and $i(M)$, along with a simple phase-shift computation, which can greatly improve the operation efficiency and is very suitable for the digital implementation. The signal amplitude of a specific frequency can be read by setting a specific k value.

Through the transformation of the induced high-frequency current components, $|i_{id''}|$ and $|i_{iq''}|$ in equation (15) could be extracted by SDFT algorithm with k being set as zero.

3. Initial Rotor Position Estimation

For synchronous motors, initial rotor position is a necessary information to ensure the effective starting. Traditional sensorless control technology based on back EMF could not obtain the initial position effectively for the back EMF which is zero when the motor is at rest. For the IPMSMs, because of their salient effect, the rotor position information is always contained in the induced high-frequency current components, with which the initial position might be obtained.

According to above analysis, the position information existing in the high-frequency current components has the form of $2\Delta\theta$, and the N/S pole could not be directly judged. In this paper, a magnetic polarity identification method is based on the amplitude variation of the same induced high-frequency current components.

According to the flux saturation effect, when the direction of induced high-frequency current vector is consistent with the N pole, the induced current's amplitude would be the largest; on the contrary, the amplitude will become the smallest when the direction is consistent with the S pole. Therefore, the N/S polarity of the rotor pole can be identified by judging the amplitude of the induced high-frequency current components, which also can be realized by SDFT algorithm.

Supposing the position of N pole is θ_N when the amplitude of the high-frequency current reaches the maximum,

this angle can be used to identify the magnetic polarity although it is quite different from the actual rotor position. In detail, if the difference between θ_N and θ' is less than 90°, θ' is the actual rotor position angle; if the difference is larger than 90°, the estimated rotor position angle θ' is at the S-pole position, and the estimated rotor position would be revised to $\theta' + 180°$. The whole diagram of the studied rotor position estimation strategy is illuminated in Figure 3.

4. Experimental Results

An experimental platform for the IPMSMs was established, as shown in Figure 4, in which the control processor is TMS320F28335. The detailed parameters of the studied IPMSM are shown in Table 1. The frequency of the injected high-frequency voltage is 1250 Hz and the amplitude is 6 V.

4.1. Signal Extraction Based on SDFT. With the injected high-frequency signal (1250 Hz, 6V), when $n = 20$ rpm, the induced stator current in a-phase stator current is shown in Figure 5(a), the induced high-frequency current components obtained from band-pass filters in a-phase and b-phase are displayed in Figure 5(b).

From Figure 5, it is obvious that the induced current components are superimposed on the stator currents. With SDFT algorithm, the extracted signals are exhibited in Figure 6.

It can be seen from the experimental results in Figure 6 that this SDFT algorithm can effectively extract the amplitudes idh and iqh of the induced high-frequency current components, and then, the corresponding square values $|i_{dh}|2$ and $|i_{qh}|2$ can be calculated to perform the position estimation.

4.2. Comparisons on the New Method and the SMO Method. To make better verification of the estimation method studied in this paper, experimental comparisons are carried out between the improved SMO method mentioned in [8] and this new estimation method.

The experiments are carried out according to the following procedures to make verifications and comparisons:

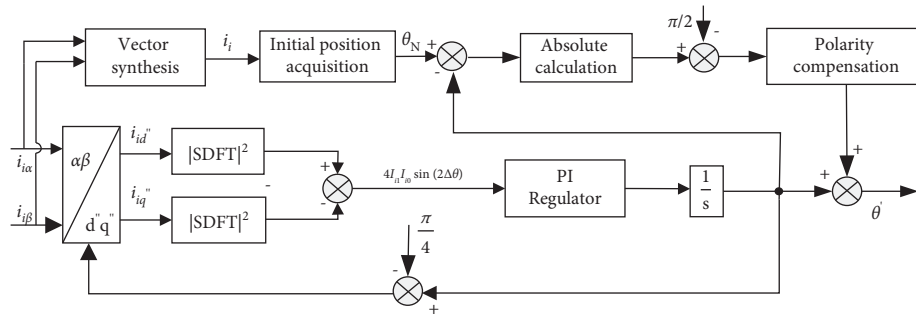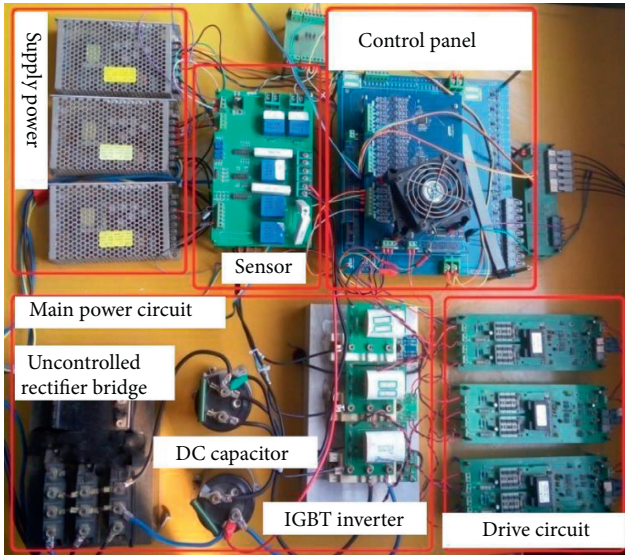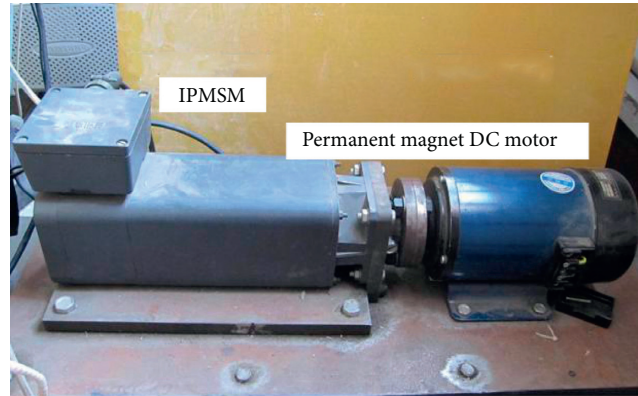(1) At $t = 0$ s, the IPMSM has a full load starting from 0 rpm to 10 rpm

FIGURE 3: Block diagram of rotor position estimation strategy.

(a)

(b)

FIGURE 4: Experimental platform: (a) main circuit and driving circuit and (b) IPMSM and the load.

TABLE 1: Detailed parameters.

Parameters	Values
PN	1.36 kW
nN	2000 r/min
TN	6.5 N.m
Rs	0.78 Ω
Ld	2.5 mH
Lq	8.5 mH
p	3
Φf	0.303 Wb
J	0.00107 kg·m^2

(2) At $t = 0.2$ s, the speed abruptly changes from 10 rpm to 50 rpm

The estimation results with the SMO method and new method are shown in Figures 7 and 8.

According to Figures 7 and 8, for the SMO method, the estimation errors are about ±6 rpm and ±4 rpm when the rotor speed is 50 rpm and 10 rpm, and the corresponding error rates are about 12% and 40%. While for this new estimation method, the estimation errors are about ±3 rpm and ±1.5 rpm and the error rates are about 6% and 15%, which fully verifies the effectiveness of the method studied in this paper.

On the contrary, the load mutation experiments are also carried out when the motor runs at 10 rpm (at $t = 0.2$ s, the load abruptly changes from 0 N·m to the rated value); the corresponding comparisons are shown in Figures 9 and 10.

According to Figures 9 and 10, when the load abruptly changes from 0 N·m to the rated value, the dynamic response times are 6.5 ms and 4.1 ms for the SMO method and new methods, respectively; for the estimation error, this new method has better performance than the conventional one, and the speed drop is about 2 rpm and 1.2 rpm, respectively. It can also be seen from Figure 10 that the estimated value differs greatly from the actual value for the SMO method has no great adaptability to the salient PMSM, and the inherent chattering characteristic of SMO also have influence on the estimation performance.

4.3. Initial Rotor Position Estimation. Taking five actual initial rotor positions, 0°, 45°, 90°, 135°, and 180°, as the tests, the trajectories of the induced high-frequency current components are presented in Figure 11, each of which is an ellipse. With the
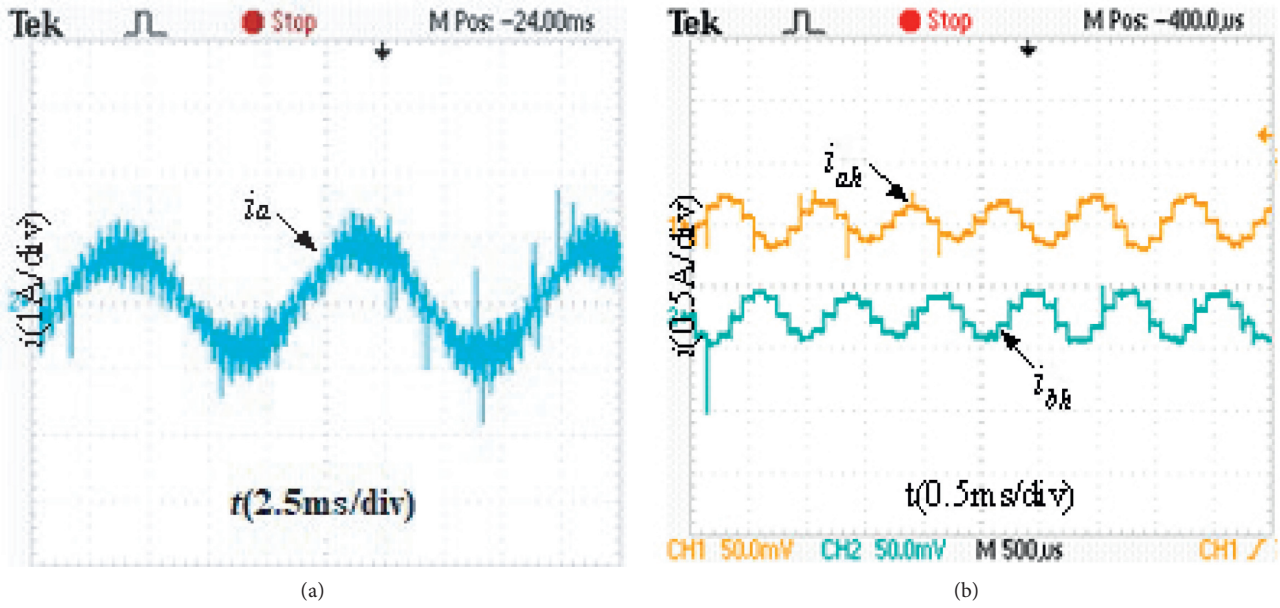
(a)

(b)

FIGURE 5: Induced high-frequency current components: (a) induced current in a-phase; (b) induced high-frequency current components.
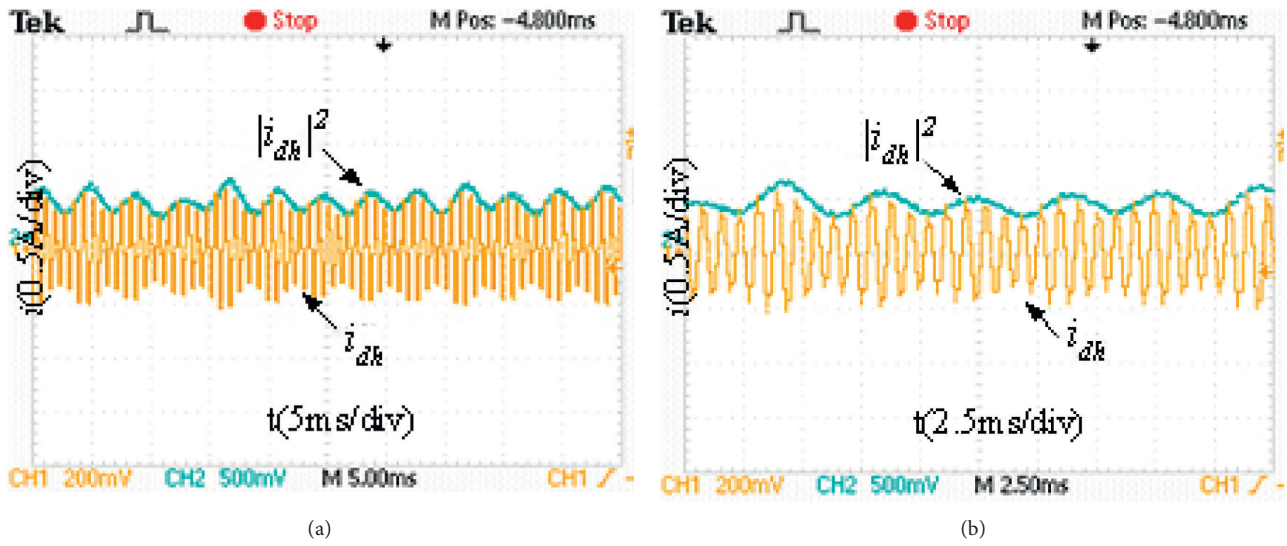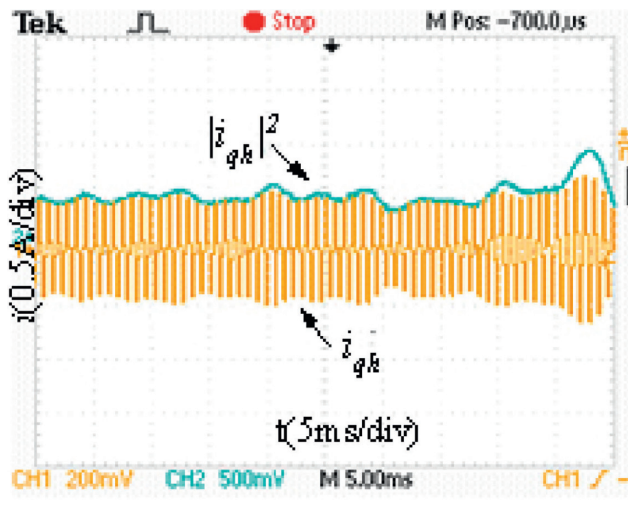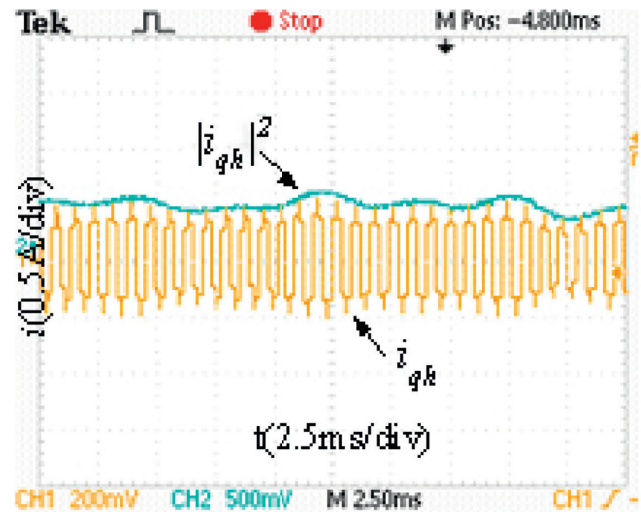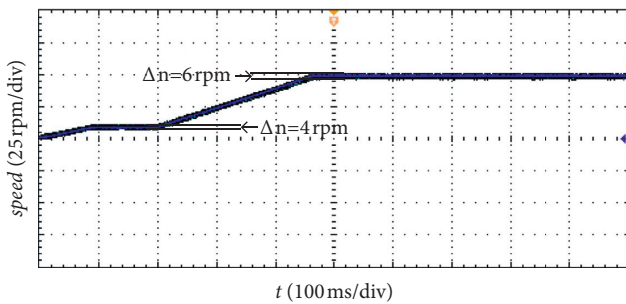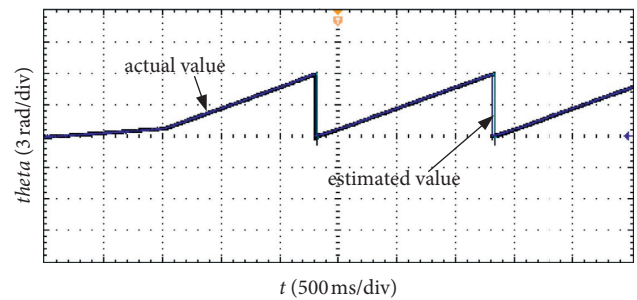

(a)

(b)

FIGURE 6: Continued.

(c)

(d)

Figure 6: Amplitudes' extraction with SDFT: (a) high-frequency current in d-axis, (b) enlarged waveforms of (a), (c) high-frequency current in q-axis, and (d) enlarged waveforms of (c).
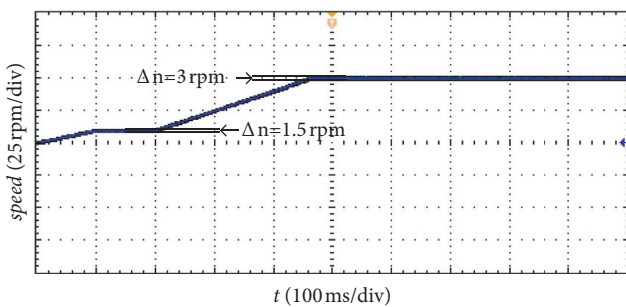

(a)

(b)

Figure 7: Estimation results of the SMO method: (a) speed estimation; (b) rotor position estimation.

(a)
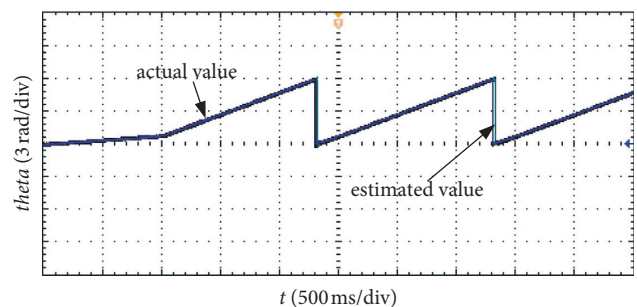
(b)

Figure 8: Estimation results of the new method: (a) speed estimation; (b) rotor position estimation.
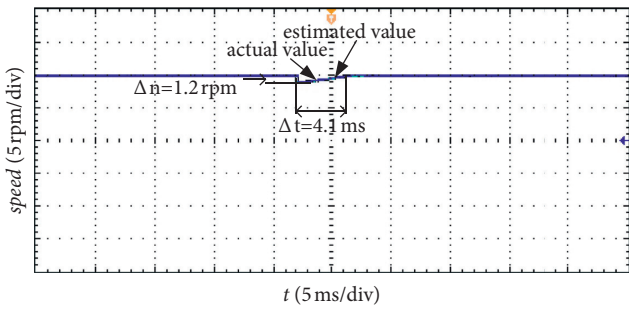
(a)
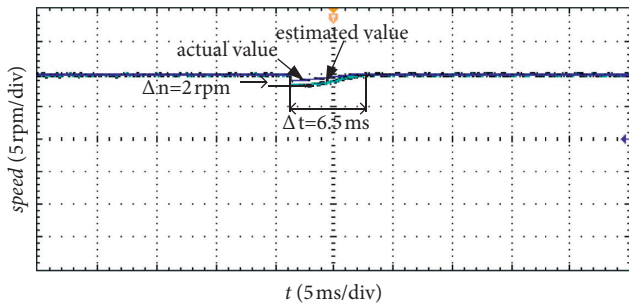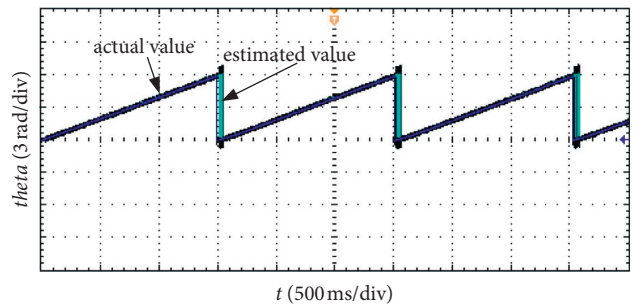
(b)

FIGURE 9: Estimation results of the SMO method: (a) speed estimation; (b) rotor position estimation.
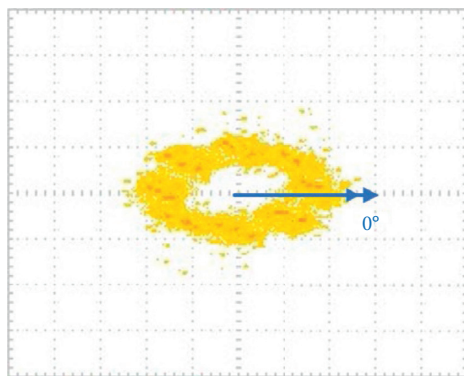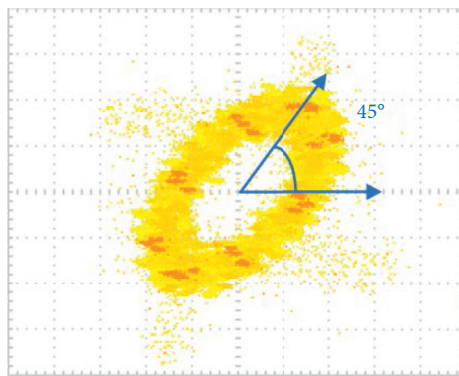

(a)
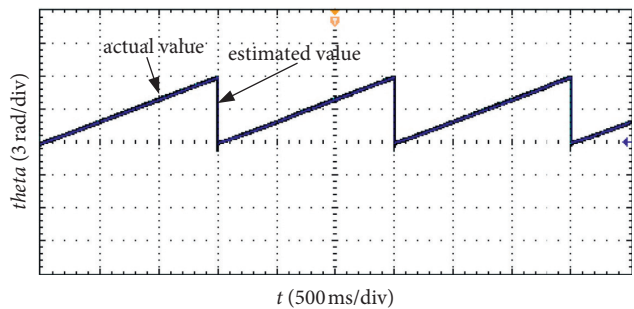
(b)

FIGURE 10: Estimation results of the new method: (a) speed estimation; (b) rotor position estimation.

(a)

(b)

FIGURE 11: Continued.
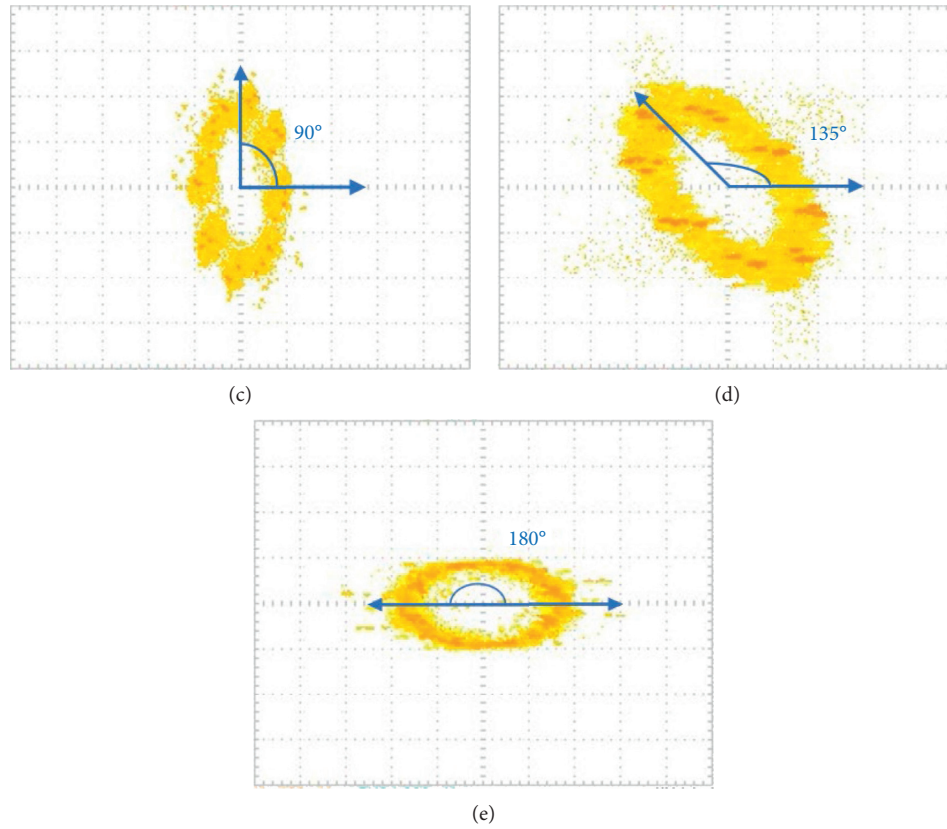
(c)

(d)

(e)

FIGURE 11: Initial rotor position estimation: (a) 0°; (b) 45°; (c) 90°; (d) 135°; (e) 180°.
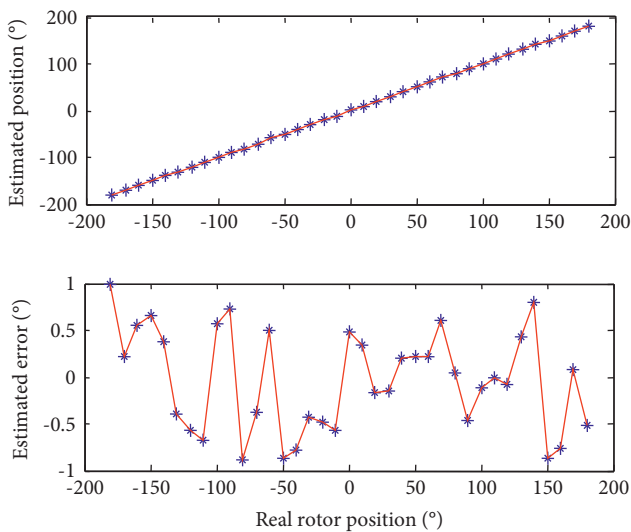

FIGURE 12: Results of the initial rotor position estimation.

proposed magnetic polarity identification method, the obtained initial rotor position could be presented as the angles between the long axis of the ellipse and the horizontal line.

Taking the actual initial rotor position as the horizontal coordinate and the estimated position and error as vertical ones, the experimental results are displayed in Figure 12, from which, it can be seen that the estimation error is within ±1°.

5. Conclusions

To effectively estimate the initial and real-time rotor positions of the IPMSMs, even a low speed situation, this paper proposed a novel estimation method with the combination of traditional high-frequency signal injection method and the SDFT algorithm. High-frequency voltage signal was injected to induce the high-frequency current components; SDFT algorithm was used to extract the amplitudes of the induced current components, with which the rotor position could be obtained in real time by a PI regulator. On the contrary, a magnetic polarity identification method was designed to get the initial position according to the amplitude variation of the induced high-frequency current components.

With this novel rotor estimation strategy, the rotor estimation accuracy can be ensured within ± 3 rpm and ± 3 rpm, even the speed is 50 rpm and 10 rpm, respectively; with the SDFT algorithm, the position extraction time reduces to about 4.1 ms which improves the dynamic performance. Besides, the initial rotor positions are well identified when the actual rotor is at different angles, which can ensure the motor having a nice starting performance.

Data Availability

The processed data required to reproduce these findings cannot be shared at this time as the data also forms part of an ongoing study.

Conflicts of Interest

The authors declare that they have no conflicts of interest.

Acknowledgments

References

[1] P. Marion, "Sensorless drives in industrial applications," *Industrial Electronics Magazine*, vol. 5, no. 2, pp. 16–123, 2011.

[2] Y. C. Kwon, S. K. Sul, N. A. Baloch, S. Moimoto, and M. Ohto, "Design, Modeling, and control of an IPMSM with an asymmetric rotor and search coils for absolute position sensorlessdrive," *IEEE Transactions on Industry Applications*, vol. 52, no. 5, pp. 3839–3850, 2016.

[3] G. Bon-Gwan, C. Jun-Hyuk, and J. In-Soung, "Development and analysis of intertum short fault model of PMSMs with series and parallel winding connections," *IEEE Transactions on Power Electronics*, vol. 29, no. 4, pp. 2016–2026, 2014.

[4] S. K. Sul, Y. C. Kwon, and Y. Lee, "Sensorless control of IPMSM for last 10 years and next 5 years," *CES Transactions on Electrical Machines and Systems*, vol. 1, no. 2, pp. 91–99, 2017.

[5] G. Wang, H. Zhou, N. Zhao, C. Li, and D. Xu, "Sensorless control of IPMSM drives using a pseudo-random phase-switching fixed-frequency signal injection scheme," *IEEE Transactions on Industrial Electronics*, vol. 65, no. 10, pp. 7660–7671, 2018.

[6] X. Song, B. Han, S. Zheng, and S. Chen, "A novel sensorless rotor position detection method for high-speed surface PM motors in a wide speed range," *IEEE Transactions on Power Electronics*, vol. 33, no. 8, pp. 7083–7093, 2018.

[7] D. Jiang, Z. Zhao, and F. Wang, "A sliding mode observer for PMSM speed and rotor position considering saliency," in *Proceedings of the IEEE Power Electronics Specialists Conference*, Rhodes, Greece, July 2008.

[8] D. Liang, J. Li, and R. Qu, "Sensorless control of permanent magnet synchronous machine based on second-order sliding-mode observer with online resistance estimation," *IEEE Transactions on Industry Applications*, vol. 3, no. 4, pp. 3672–3682, 2017.

[9] Q. Tang, A. Shen, X. Luo, and J. Xu, "PMSM sensorless control by injecting HF pulsating carrier signal into ABC frame," *IEEE Transactions on Power Electronics*, vol. 32, no. 5, pp. 3767–3776, 2017.

[10] S. I. Kim, J. H. Im, E. Y. Song, and R. Y. Kim, "A new rotor position estimation method of IPMSM using all-pass filter on high-frequency rotating voltage signal injection," *IEEE Transactions on Industrial Electronics*, vol. 63, no. 10, pp. 6499–6509, 2016.

[11] X. Zhang, H. Li, S. Yang, and M. Ma, "Improved initial rotor position estimation for PMSM drives based on HF pulsating voltage signal injection," *IEEE Transactions on Industrial Electronics*, vol. 65, no. 6, pp. 4702–4713, 2018.

[12] E. Jacobsen and R. Lyons, "The sliding DFT," *IEEE Signal Processing Magazine*, vol. 20, no. 2, pp. 74–80, 2003.

[13] H. Liu, H. Hu, H. Chen, Li Zhang, and Y. Xing, "Fast and flexible selective harmonic extraction methods based on the generalized discrete Fourier transform," *IEEE Transactions on Power Electronics*, vol. 33, no. 4, pp. 3484–3496, 2018.

[14] Q. Yuan, Y. Yang, H. Wu, and H. Wu, "Low speed sensorless control based on an improved sliding mode observation and the inverter nonlinearity compensation for SPMSM," *IEEE Access*, vol. 8, pp. 61299–61310, 2020.

[15] X. Sun, L. Chen, Z. Yang, and H. Zhu, "Speed-sensorless vector control of a bearingless induction motor with artificial neural network inverse speed observer," *IEEE*, vol. 18, no. 4, pp. 1357–1366, 2013.

[16] X. Sun, J. Cao, G. Lei, Y. Guo, and J. Zhu, "Speed sensorless control for permanent magnet synchronous motors based on finite position set," *IEEE Transactions on Industrial Electronics*, vol. 99, p. 1, 2019.

[17] Yu-seok Jeong, R. D. Lorenz, M. Thomas, and Jahns, "Initial rotor position estimation of an interior permanent-magnet synchronous machine using carrier-frequency injection methods," *IEEE Transactions on Industry Applications*, vol. 41, no. 1, pp. 38–45, 2005.